Flame Retardant Behavior of Polyelectrolyte–Clay Thin Film Assemblies on Cotton Fabric

Yu-Chin Li,[†] Jessica Schulz,[†] Sarah Mannen,[†] Chris Delhom,[‡] Brian Condon,[‡] SeChin Chang,[‡] Mauro Zammarano,[§] and Jaime C. Grunlan[†,*]

[†]Department of Mechanical Engineering, Materials Science and Engineering Program, Texas A&M University, College Station, Texas 77843, [‡]Southern Regional Research Center, USDA-ARS, 1100 Robert E. Lee Boulevard, New Orleans, Louisiana 70124, and [§]Fire Science Division, Building and Fire Research Laboratory, National Institute of Standards and Technology, Gaithersburg, Maryland 20899

ABSTRACT Cotton fabric was treated with flame-retardant coatings composed of branched polyethylenimine (BPEI) and sodium montmorillonite (MMT) clay, prepared *via* layer-by-layer (LbL) assembly. Four coating recipes were created by exposing fabric to aqueous solutions of BPEI (pH 7 or 10) and MMT (0.2 or 1 wt %). BPEI pH 10 produces the thickest films, while 1 wt % MMT gives the highest clay loading. Each coating recipe was evaluated at 5 and 20 bilayers. Thermogravimetric analysis showed that coated fabrics left as much as 13% char after heating to 500 °C, nearly 2 orders of magnitude more than uncoated fabric, with less than 4 wt % coming from the coating itself. These coatings also reduced afterglow time in vertical flame tests. Postburn residues of coated fabrics were examined with SEM and revealed that the weave structure and fiber shape in all coated fabrics were preserved. The BPEI pH 7/1 wt % MMT recipe was most effective. Microcombustion calorimeter testing showed that all coated fabrics reduced the total heat release and heat release capacity of the fabric. Fiber count and strength of uncoated and coated fabric are similar. These results demonstrate that LbL assembly is a relatively simple method for imparting flame-retardant behavior to cotton fabric. This work lays the foundation for using these types of thin film assemblies to make a variety of complex substrates (foam, fabrics, *etc.*) flame resistant.

KEYWORDS: layer-by-layer assembly · clay · nanocomposites · vertical flame test · flame retardant · cotton fabric

Fire has been a useful tool throughout human history, but it can also bring disaster if not carefully controlled. In the United States, fire has killed more people than all natural disasters combined. According to a report from the National Fire Protection Association (NFPA), there were an estimated 1.6 million fires in 2007 that resulted in 3430 civilian deaths, 17 675 injuries, and the loss of 118 firefighters. Direct property loss due to fires was estimated at $14.6 billion.[1] A wide range of commonly used materials are flammable, which means the use of flame retardants can diminish these hazards and significantly contribute to saving lives and resources. The recent loss of a university student, whose clothing caught fire during a laboratory experiment, was a stark reminder of the need to reduce clothing flammability.[2] By slowing down the burning process there is a better chance for people to escape uncontrolled fires and fire-fighters to extinguish them before they cause significant damage.

Cotton is one of the most important natural textile fibers used to produce apparel, home furnishings, and industrial products, but this cellulosic material has a low limiting oxygen index (LOI) and combustion temperature (360–425 °C) that makes it highly flammable.[3] Cotton textiles burn rapidly once ignited, and the flame spreads quickly, potentially causing fatal burns within 15 s of ignition.[4] Various methods have been used to modify the combustion characteristics of textiles, including cotton. Halogenated and boron-containing additives are widely used to exclude oxygen by generating large volumes of nonflammable gases and forming a glass coating during thermal decomposition.[4,5] Despite their effectiveness, the halogenated flame retardants have been reported to form toxins that can be harmful to humans and the environment. Boron-containing flame retardants are limited by their lack of durability, which restricts them to nonaqueous washing.[3] Durable phosphorus-based treatments are currently the most successful, commercially useful flame retardants. These coatings are able to withstand repeated wash cycles,[3] reduce volatile fuel, lower pyrolysis temperature, increase carbonaceous char, and decrease afterglow.[6] Cross-linking has been used to improve phosphorus durability, but this adversely affects mechanical properties, such as tensile strength, and can create undesirable stiffness.[7] Recently, it was reported that the presence of montmorillonite (MMT) clay mixed into polymeric materials can reduce flammability and increase heat

*Address correspondence to jgrunlan@tamu.edu.

Received for review December 10, 2009 and accepted May 17, 2010.

Published online May 24, 2010.
10.1021/nn100467e

resistance at very low loadings (2−5 wt %).[8,9] Nylon, polypropylene, and polylactide have been hybridized with clay to produce nanocomposite textile fabrics, and their fire performance is improved compared to the virgin polymeric fibers.[8−10] Some of the flame-retardant nanocomposite coatings applied onto cotton fabrics include polyurethane (PU)/MMT and PU/polyhedral oligomeric silsesquioxane (POSS),[11] as well as carbon nanotubes.[12] Although these PU coatings show reduced heat release, they involve a complex two-stage synthesis. As for the carbon nanotubes, although they improve flame retardancy and other functionalities, high cost and the resulting opaqueness (blackness) will likely limit their prospects for commercialization.

It has been proposed that the combustion process in polymer/clay systems involves a protective charred ceramic surface layer that is created during polymer ablation. Such a layer is presumably formed by the reassembly of the finely dispersed clay, which results in 70 to 80% reduction in heat release for nanocomposites made at low clay loadings (typically 2 to 5 wt %).[13] Nanotubes have shown similar behavior by a similar mechanism.[14] It is this ceramic char-layer silicate nanocomposite theory of fire-retardance that inspired the use of layer-by-layer (LbL) assembly to create densely layered nanocomposites in an effort to produce more flame-retardant materials.

Since the early 1990s, layer-by-layer assembly has been studied extensively and is a relatively simple technique to fabricate multifunctional thin films that are typically less than one micrometer thick.[15−18] The most common method for LbL assembly consists of alternately dipping a substrate into positively and negatively charged, dilute (<1 wt % solids), aqueous solutions/mixtures of polymers or particles, and building up multiple positive/negative pairs of layers (also known as bilayers [BL]), exploiting the electrostatic attractions between layers to hold the film assembly together. Electrostatic interactions are not the only intermolecular binding force used for assembly, as these multilayered films have been assembled *via* hydrogen bonding,[19,20] donor/acceptor interactions,[21] and covalent bonds.[22,23] Formulation and process conditions such as chemistry of the layer components,[24,25] counterions,[24] molecular weight,[26] ionic strength,[27] and pH[28,29] of the dipping solutions/mixtures, and temperature,[28,30] can influence BL thickness, which typically ranges from 1−100 nm. Recent studies on a variety of LbL films highlight a diverse and useful set of properties that include antimicrobial,[31,32] antireflection,[33] and electrochromic,[34−36] as well as potential applications ranging from drug delivery,[37] to oxygen barrier,[38] to sensors.[39−41] In many cases it is the presence of nanoparticles within the film, such as clay,[38,42−45] which imparts the desired property.

The use of sodium montmorillonite (MMT) clay in LbL thin films has been well-studied.[38,46,47] An individual MMT clay platelet (approximately one nanometer thick) is composed of two tetrahedral Si^{4+} layers intercalated by an octahedral Al^{3+} or Mg^{2+} layer in between. It has swelling and ion exchange properties, allowing for exfoliation of the platelet and for its surface to become negatively charged when immersed in water.[42] It is these negatively charged surfaces that allow MMT platelets to be incorporated into LbL assemblies when paired with a positively charged ingredient. Previous work has shown that Laponite synthetic clay, can impart some modest flame-retardance to cotton fabrics *via* LbL assembly.[48] In the present work, MMT was deposited with branched polyethylenimine (BPEI) to generate nanocomposite assemblies on cotton fibers. The thickness and weight composition of these films was tailored by changing the pH of the polymer solution and the concentration of the clay mixture. Four different BPEI-MMT formulations were applied to cotton fabric and the flame-retardant properties were studied by thermogravimetric analysis (TGA), vertical flame testing, and microcombustion calorimetry. Additionally, the mechanical properties and water-wicking ability of the coated fabrics were also examined. High assembly pH and clay concentration resulted in fabric with the best flame resistance. Five BL of pH 10 BPEI and MMT (0.1 and 1 wt % in water) added 2 wt % to the cotton fabric, which maintained 11% of its weight at 500 °C and a significant level of fiber and fabric weave structure was maintained following vertical burn. This study represents the first in-depth study of an LbL-based flame retardant. The use of MMT is a dramatic improvement over the much smaller Laponite,[48] which was used in the only other mention of layer-by-layer assembly for imparting flame resistance to fabric. A framework is provided for improving the antiflammability of cotton (and other flammable materials such as foam insulation) that could result in significant savings of both life and property.

RESULTS AND DISCUSSION

Growth and Structure of Polymer/Clay Assemblies. The influence of pH and concentration of the deposition mixtures on the growth of the thin films was evaluated by ellipsometry. Four different thin film recipes, BPEI pH 7 or 10, with MMT at 0.2 wt % or 1 wt %, were used to prepare the films whose growth is shown in Figure 1. All four systems grow linearly as a function of BPEI-MMT bilayers deposited. The film thicknesses are very similar for films made with the same pH BPEI solution, regardless of variation in clay concentration. Differences observed between high and low pH systems are due to the different degrees of charge density of the weak polyelectrolyte BPEI. When this polymer is highly charged, the polymer chains adopt a flat conformation due to self-repulsion of like charges along its backbone, whereas at low charge density, the polymer has a more coiled and bulky conformation due to intrachain

H-bonding.[29] These results agree with growth trends observed in a recent study of a nearly identical system focused on oxygen barrier behavior of clay-based assemblies, where dip times were 1 minute rather than 2.[38] In order to better understand this growth process, a quartz crystal microbalance was used to measure the weight increase associated with the deposition of each individual layer.

Figure 2 shows the QCM data for the four different recipes described above. There is not much difference observed in mass per layer of films made with pH 7 BPEI and the two different concentrations of MMT suspensions (0.2 and 1 wt %), but the films made with pH 10 BPEI and two different concentrations of MMT show a significant difference in mass. The amount of BPEI deposited for each layer is similar between the films made with the same pH, but BPEI at pH 7 deposits less in each layer than BPEI pH 10 (about one-third the amount). The films made with 1 wt % MMT suspension and BPEI at different pH values have higher clay loadings (MMT/BPEI ratio) than films made with 0.2 wt % MMT suspension (data not shown). In all four recipes, film thickness seems to be influenced primarily by the pH of the BPEI solution and only modestly by the concentration of clay. However, film weight is a different story. As mentioned above, when BPEI has a higher charge density (at low pH), it lies flatter on the charged substrate due to intrachain self-repulsion, and the clay platelets can only lay parallel to the substrate, covering the topmost surface. In this case, films made with a 1 wt % MMT mixture would achieve better coverage per deposition than films made with 0.2 wt % MMT, resulting in similar thicknesses and weights for the two films. On the other hand, when BPEI has a lower charge density (at pH 10), it is more coiled and entangled than in its high charge density state, This results in thicker, rougher layer deposition that would conceivably allow for more clay platelets to deposit due to the greater surface area of this relatively coarse (on the nanoscale) surface. In this scenario, a higher concentration of MMT (1 wt %) could result in more loading of the BPEI surface during each deposition step than the more dilute mixture (0.2 wt % MMT).

Tapping mode AFM was used to characterize the surfaces of 30 BL MMT-composite thin films made with high and low pH BPEI. The root-mean-square (rms) roughness (using a 20 μm square area) for the BPEI pH 7/1 wt % MMT film is 38 nm (Figure 3a,b), while it is 62 nm for the BPEI pH 10/1 wt % MMT film (Figure 3c,d), suggesting that the surface is covered by clay platelets whose largest dimension is oriented parallel to the surface of the silicon substrate. Because of the different morphology of BPEI at high and low charge densities, the surface is rougher for films made with pH 10 BPEI that has little charge. Figure 3e shows a TEM cross-section of a 40 BL film made with BPEI pH 10/0.2 wt % MMT, to provide some idea of structure through the

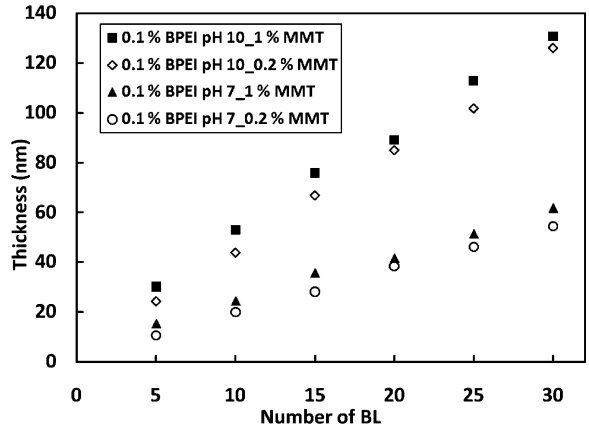

Figure 1. Film thickness as a function of the number of bilayers deposited, for a series of LbL assemblies made with varying pH of the BPEI solution and concentration of the MMT mixture. MMT was used at its unadjusted pH of 9.8.

thickness of these films. This film was deposited on a polystyrene substrate to facilitate sectioning. The individual layered clay can be seen very clearly, as well as the places where the clay platelets meet. The film appears wavy in the images, which was likely caused by stress relaxation in the film during sectioning with a diamond knife and/or because of the tilted layers of clay.[49] Even so, the nano-brick-wall structure of these films is very evident. It is this unique nanostructure that is believed to provide flame resistance to cotton fabric.

Flame Resistance of Fabric. Cotton fabric was coated with 5 and 20 BL of BPEI/MMT, using the four different recipes described in the previous section describing thin film growth. The coating weight was determined by weighing 12 by 15 in. samples of fabric before and after coating. All samples were weighed only after oven-drying at 80 °C for 2 h to remove moisture. Weight added to the fabric by each coating system is shown in Table 1 as a percentage of the uncoated weight. The weight gain from coating on fabric does not correlate well to the weight gain measured by QCM for the films assembled on a quartz crystal. At 5 BL, fabric coated

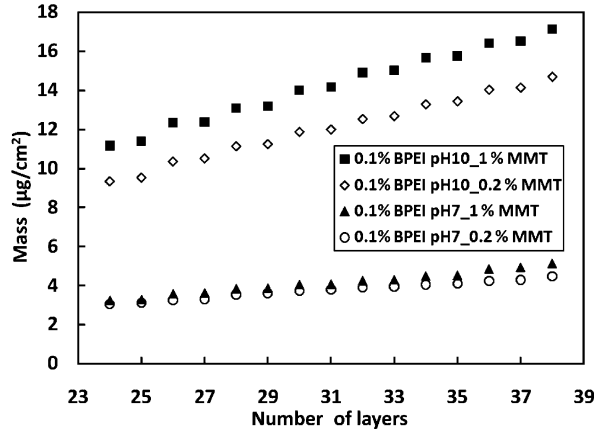

Figure 2. Film mass as a function of individually deposited clay and polymer layers for four different BPEI/MMT systems. In all cases, odd layers are BPEI and even layers are MMT.

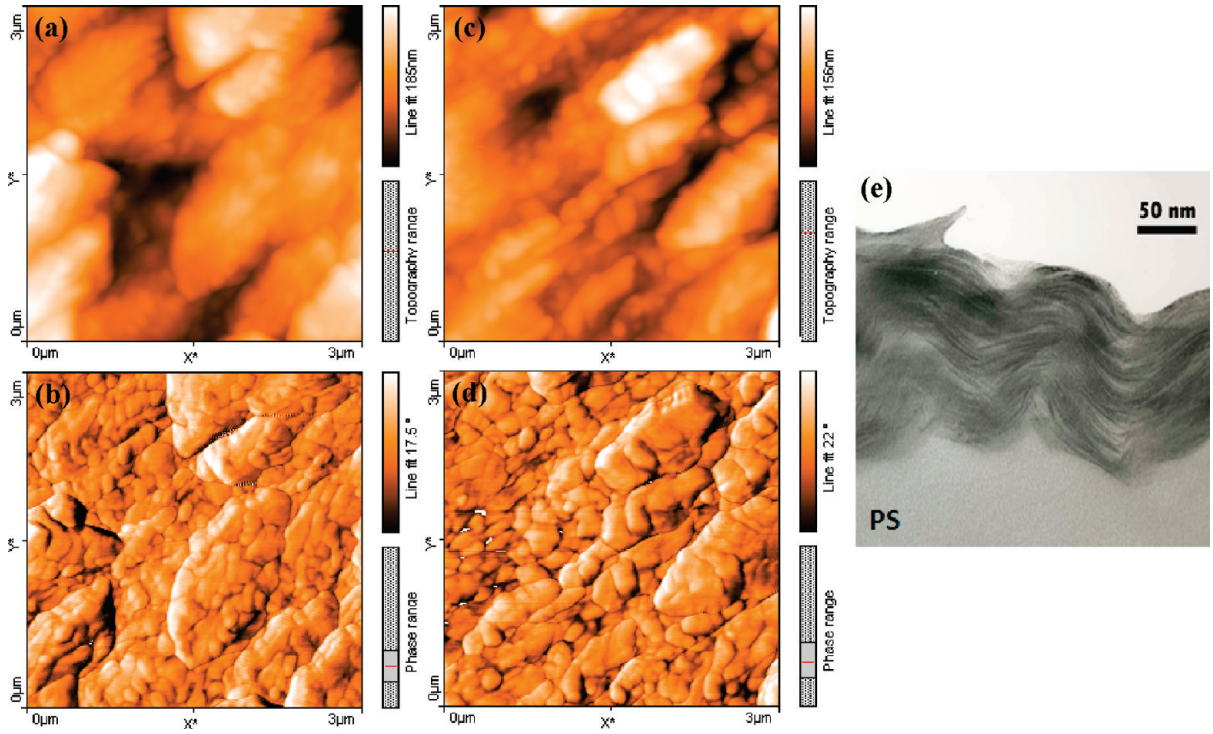

Figure 3. AFM height (a) and phase (b) surface images of a 30 BL BPEI pH 10/1 wt % MMT film; height (c) and phase (d) images of a 30 BL BPEI pH 7/1 wt % MMT film; and TEM cross-section (e) of a 40 BL assembly made with BPEI pH 10/0.2 wt % MMT. The TEM image (e) is reprinted from ref 38. Copyright 2010 American Chemical Society.

using BPEI at pH 10 is heavier than fabric coated using pH 7 BPEI, but at 20 BL the fabric weight gain was greater with pH 7 BPEI. This may be linked to differences in adhesion and substrate geometry. Figure 4 shows two coatings that were prepared using a 1 wt % MMT mixture with BPEI at high and low pH. All of the individual cotton fibers are easily discerned for the 20 BL coating made with BPEI at pH 10 (Figure 4a). The same coating applied using BPEI at pH 7 (Figure 4b) appears to have pulled away from the fiber to some extent during the deposition process, which allowed it to bridge multiple fibers. It is likely that coating draped between fibers provided additional surface area for deposition, which resulted in a greater add-on percent at 20 BL.

Figure 5 shows TGA results for each of four coating recipes at 5 (Figure 5a) and 20 BL (Figure 5b). At 500 °C, under an air atmosphere, the uncoated control fabric left less than 1.8 wt % residue. With the addition of 2 wt % for a 5 BL coating and 4 wt % for a 20 BL coating, residue weight percentages for the coated fabrics are 1 order of magnitude higher than that of the control. The residue amounts for the control fabric and each coated fabric are summarized in Table 1. At the final stage of the testing (around 600 °C), there was essentially no char left from the control fabric, but there was a significant amount of residue left from 20 BL-coated fabrics. The mass of the residue from a coated fabric clearly demonstrates that there is preservation of cotton during burning, because some residues are greater than the mass of the coating itself (see add-on % in Table 1). The amount of charred cotton in the residue is higher than the mass difference between residue and the coating by itself (in all cases), because at least a fraction of the BPEI in the coating is degraded during heating (pure BPEI completely decomposes below 650 °C). It should be noted that there is a direct correlation between added coating weight (Table 1) and residue generated in the TGA. Additionally, the fiber bridging and heavier coverage by the pH 7 BPEI sys-

TABLE 1. Weight Added by Coating Fabrics, and Residue Amounts after Heat Treatment[a]

	add-on (%)		500 °C residue (%)		600 °C residue (%)	
sample	5 BL	20 BL	5 BL	20 BL	5 BL	20 BL
control			1.77[b]		0.30[b]	
BPEI pH10/0.2% MMT	2.05	2.31	9.12	11.70	1.29	2.09
BPEI pH 7/0.2% MMT	0.97	2.89	7.00	10.39	1.17	3.28
BPEI pH10/1% MMT	2.23	4.06	11.26	12.16	1.70	2.82
BPEI pH 7/1% MMT	1.82	4.41	9.33	13.02	1.47	4.72

[a]Residue values obtained from TGA testing under air atmosphere. [b]The residue weight percent of uncoated fabric.

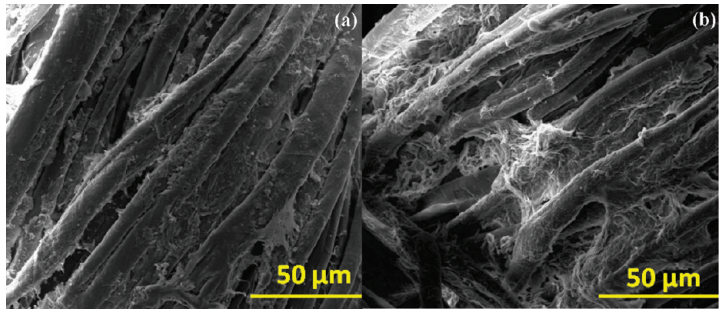

Figure 4. SEM images of cotton fabric coated with 20 BL of BPEI/MMT. These coatings were made using BPEI at pH 10 (a) and 7 (b). Both coatings were prepared with a 1 wt % MMT deposition mixture.

tem at 20 BL (Figure 4) results in 10% greater coating weight, but 67% greater char at 600 °C.

An equivalent set of coated fabric samples was put through vertical flame testing (ASTM D6413). Time to ignition did not increase upon coating the fabric, but a brighter and more vigorous flame was observed on the control fabric compared to the coated fabrics, as shown in Figure 6 at 5 s after ignition. The flame on the coated fabric was not very vigorous. Additionally, more glow was seen on the control fabric after the flame was removed. The control and eight different coated fabrics showed similar after-flame times (i.e., time fire observed on samples after direct flame removed), but the afterglow times for coated fabrics were 9 s less than for the uncoated fabric. After burning, no control fabric was left on the sample holder, but all four 20 BL-coated fabrics left significant residues, as shown in Figure 7 (see Supporting Information for images of the residues of 5 BL-coated fabrics). The residues from 20 BL-coated fabrics are heavier and have preserved the fabric structure bet-

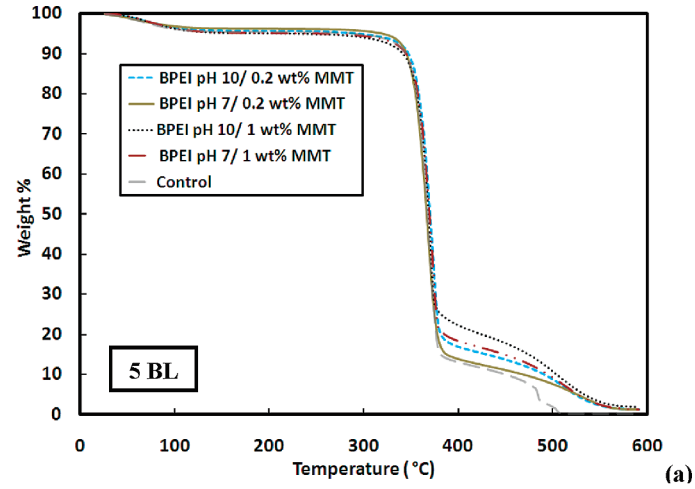

Figure 5. Weight loss as a function of temperature for cotton fabrics coated with 5 BL (a) and 20 BL (b) of 0.1 wt % BPEI (pH 10 and 7) with 0.2 and 1 wt % MMT. These results were obtained using TGA at a heating rate of 20 °C/min under an air atmosphere.

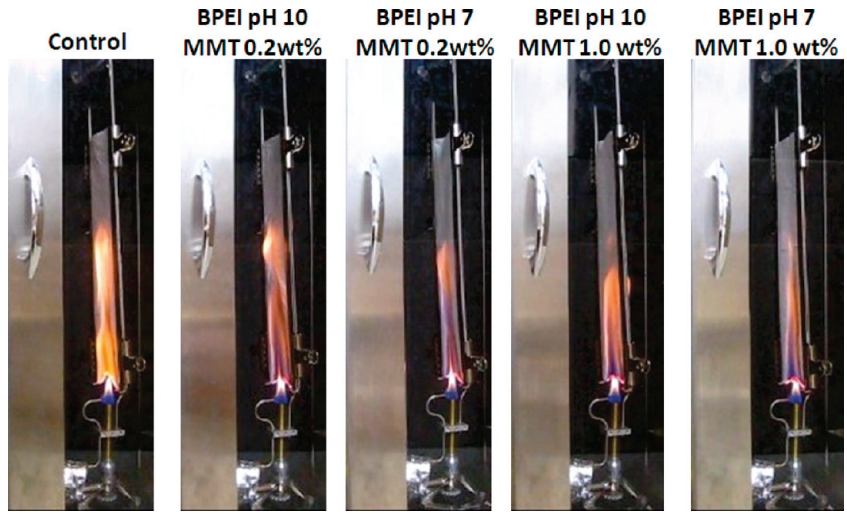

Figure 6. Images of vertical flame testing of the uncoated and coated cotton fabrics 5 s after ignition. The coated fabrics are 20 BL of a given recipe.

ter than the residues from fabrics coated with only 5 BL, although even these thinner coating provide significant char.

All fabrics were imaged by scanning electron microscopy, before and after flame testing, to evaluate the surface morphology and fabric structure. The control fabric left only ash after flame exposure, so these ashes were used for imaging, whereas coated fabric images are more representative from the center of the charred remains. In Figure 8a,b, the uncoated and 5 BL (BPEI pH 10/0.2 wt % MMT)-coated fabrics are shown prior to the flame test. The fiber surface in the control fabric appears very clean and smooth compared to the coated fabrics. Small MMT aggregates can be seen on the fibers of the coated fabrics that are likely the result of inefficient rinsing of fabric between layers. Each fiber of the fabric is at least partially, if not completely, covered by the clay coating. After flame testing, the ash from the uncoated fabric and the residue from coated fabric were imaged under the same magnification. Figure 8c very clearly shows that the ashes of the uncoated cotton fabric no longer have the same fabric structure and shape of the original fibers. Broken pieces and holes in the fiber strands illustrate the complete destruction that occurs during burning of uncoated cotton. It is surprising that with only 5 BL, the fabric structure is maintained and the fibers are relatively intact (Figure 8d). It is possible that during burning at high temperature, the MMT platelets fuse together to some extent, which could account for not seeing aggregated MMT or the edges of the platelets after burning, but rather large continuous pieces of coating instead.

Figure 9a shows a low magnification image of the fabric before burning, coated with 5 BL of BPEI pH 7/1 wt % MMT. The dimensions of the weave structure in uncoated and coated fabrics are identical, which means that the LbL coating process does not alter the fabric dimensions. After burning, ash remaining from the uncoated fabric does not show the weave structure anymore (Figure 9b), but the residue from coated fabrics retain the weave structure, especially with a 20 BL coating of BPEI pH 7/1 wt % MMT (Figure 9d). Even the width of individual yarns is similar to the width before burning for this sample. The 5 BL (BPEI pH 7/1 wt %

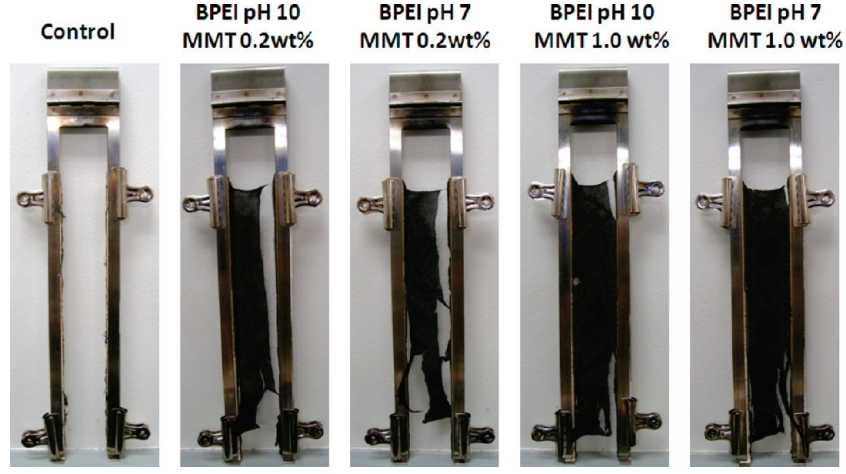

Figure 7. Images of uncoated and 20 BL-coated cotton fabrics following the vertical flame test.

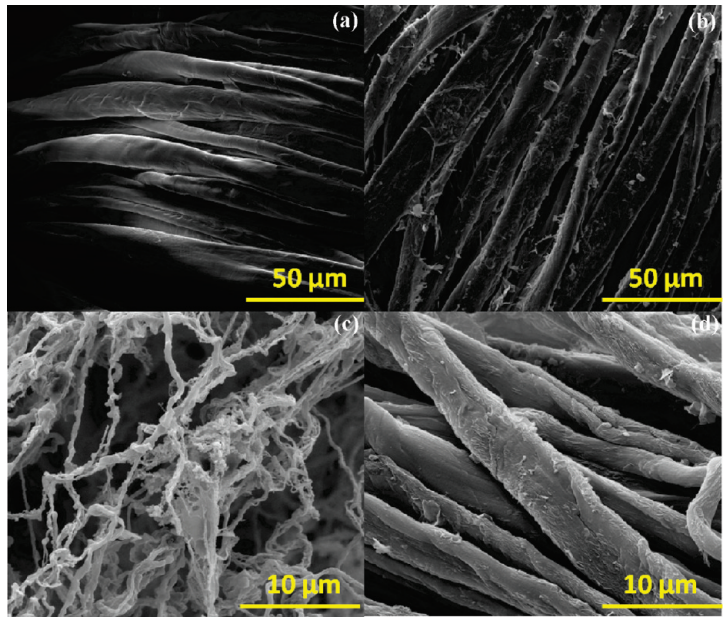

Figure 8. SEM images of uncoated fabric before (a) and after (c) the vertical flame test. Five BL-coated fabric (BPEI pH 10/ 0.2 wt % MMT) before (b) and after (d) flame test is also shown.

MMT)-coated fabric also retained its weave structure (Figure 9c), although the threads shrank after flame testing, leaving gaps between the yarns. Interestingly, despite using the same concentration of clay deposition mixture (1 wt % MMT), the weave structure of the residue from 20 BL-coated fabric made using pH 10 BPEI (Figure 9e) has larger gaps between yarns as compared to the fabric coated (20 BL) using pH 7 BPEI. This is a somewhat expected result due to the smaller add-on percentage of the BPEI pH 10 coating, as well as to the fiber bridging, achieved by the coating when highly charged pH 7 BPEI is used (see Table 1 and Figure 4), which may have provided greater barrier to fibers deeper within the fabric.

The XRD pattern in Figure 10 provides additional evidence of coating on the fabric. The low-angle peak at 7.8° for neat MMT clay derives from a basal spacing of 11.4 Å, which is the periodic distance from platelet to platelet. On the fabric coated with BPEI pH 7/1 wt % MMT, the peak is shifted to 6.4°, suggesting that even on the nonflat fiber surface the clay can be deposited in an orderly manner. The basal spacing is increased to 13.7 Å because of intercalation with BPEI. After vertical flame testing, the residue from coated fabric was also scanned by XRD, which resulted in a decrease from 13.7 to 12.7 Å. This result suggests that the intercalated BPEI is decomposed or ablated during the burning process, resulting in a reduction of the basal spacing of MMT. The positions of the low-angle MMT peak (data not shown) of fabric coated with BPEI pH 10/1 wt % MMT (before and after flame test) show no significant difference between the two recipes.

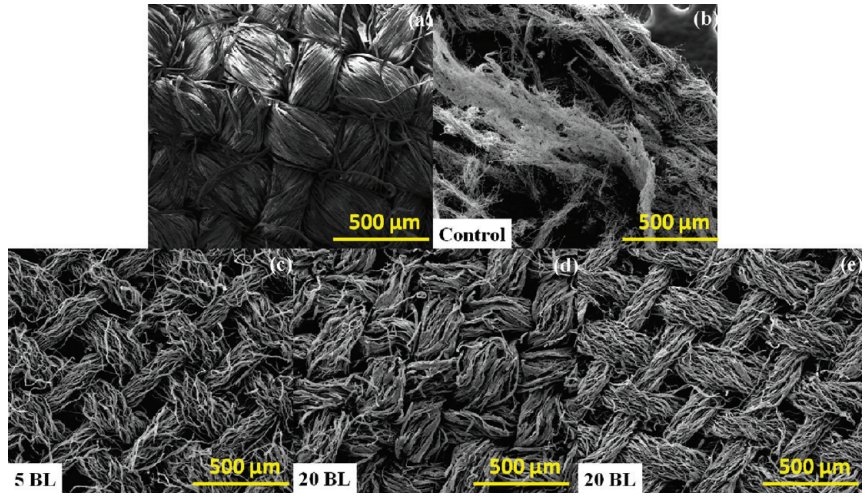

Figure 9. Low magnification SEM images highlighting the weave structure of fabrics before and after burning: coated fabric before burning (a), ash from control fabric after burning (b), residues from fabric coated with 5 (c), and 20 BL (d) of BPEI pH 7/1 wt % MMT, and residue from fabric coated with 20 BL of BPEI pH 10/1 wt % MMT (e).

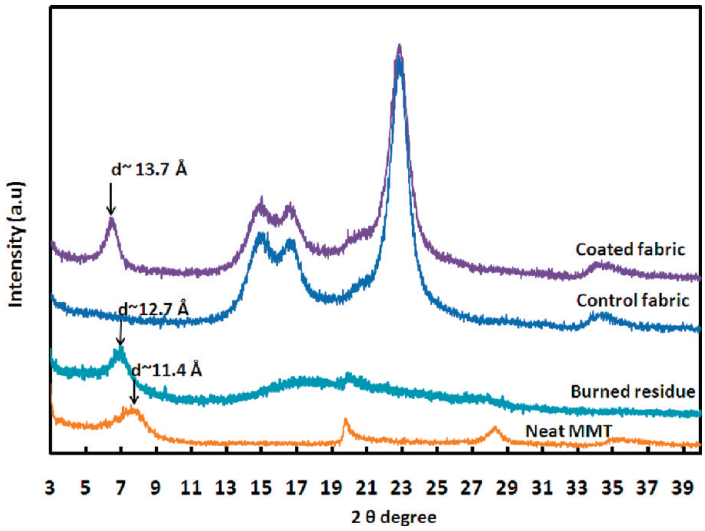

Figure 10. X-ray diffraction patterns for neat MMT, 20 BL BPEI pH 7/1 wt % MMT coated fabric, before and after burning, and the control fabric.

Another tool for assessing the fire behavior of small (mg) samples is the microscale combustion calorimeter (MCC). The MCC simulates the burning process by using anaerobic pyrolysis and a subsequent reaction of the volatile pyrolysis products with oxygen under high temperatures to simulate surface gasification and flaming combustion.[50] Both heat release rate and temperature as a function of time at constant heating rate are measured during the test.[51] Key parameters coming from the MCC test include temperature at maximum heat release rate (T_p), specific heat release rate (HRR in W/g) (that is obtained by dividing the heat release rate at each point in time by the initial sample mass), and total heat release (THR in kJ/g) from combustion of the fuel gases per unit mass of initial sample (obtained by time-integration of HRR over the entire test). Residue is calculated by weighing the sample before and after the test. A derived quantity, the heat release capacity (HRC in J/(g K)) is obtained by dividing the maximum value of the specific heat release rate by the heating rate during the test. HRC is a molecular level flammability parameter that is a good predictor of flame resistance and fire behavior when only research quantities are available for testing. Reproducibility of the test for homogeneous samples is about ±8%.[52]

MCC data for the coated fabric samples are summarized in Table 2. All residues from coated fabrics tested at 700 °C under nitrogen atmosphere are higher than those from uncoated fabric. The residue does not come only from the coating (see add-on wt% in Table 1), but rather the fabric itself was somewhat preserved (1−5 wt %) when coated with various recipes. These results suggest that clay surrounds each fiber and acts as a protective barrier capable of promoting char formation during the pyrolysis of the fabric. An increase in charring induces a decrease in the amount and rate of combustible volatile release, resulting in lower flammability (as evidenced by lower THR and HRC values in the MCC). The maximum reduction in THR (20%) and HRC (15%), as compared to the control, is observed in the fabric coated with 5 BL of BPEI pH10/1 wt % MMT. Increasing the number of BL up to 20 for the same sample does not appear to produce any significant variation in the MCC data. This suggests that a 5 BL coating may be sufficient for generating an effective fire barrier on the textile. An increase in T_p is also observed in all coated fabrics, which is likely due to the formation of a low permeability barrier that delays the release of combustible volatiles.

TABLE 2. Microscale Combustion Calorimeter Results for Various Coated Fabrics

sample	residue (%)	HRC (J/(g K))	THR (kJ/g)	T_p (°C)
control	2.88 ± 0.40	273.67 ± 25.38	11.63 ± 0.21	369 ± 0.58
BPEI pH 10/0.2% MMT				
5 BL	6.38 ± 1.50	254.33 ± 25.01	11.23 ± 0.25	374 ± 0.58
20 BL	7.48 ± 0.50	250.33 ± 14.50	11.10 ± 0.36	376 ± 2.65
BPEI pH 7/0.2% MMT				
5 BL	6.75 ± 0.60	260.33 ± 4.04	11.17 ± 0.40	376 ± 2.00
20 BL	6.74 ± 0.20	286.33 ± 8.51	11.90 ± 0.36	369 ± 0.58
BPEI pH10/1% MMT				
5 BL	10.52 ± 0.30	220.00 ± 6.08	9.87 ± 0.31	382 ± 0.58
20 BL	10.49 ± 0.50	221.30 ± 7.57	10.23 ± 0.06	380 ± 0.58
BPEI pH 7/1% MMT				
5 BL	8.37 ± 0.50	251.30 ± 10.02	10.73 ± 0.25	379 ± 1.00
20 BL	10.54 ± 0.30	240.30 ± 11.37	10.70 ± 0.50	377 ± 2.65

Physical Properties of Fabric. There is no difference in appearance between coated and uncoated fabric. Even tactile assessment of the fabric (by touch of hand) is the same for all coated and uncoated samples tested. In many cases the addition of a flame retardant results in loss of strength or the degradation of other fabric properties (*e.g.*, moisture wicking), so it is important to know if this coating technology alters these properties. Fabric count, tear and tensile strength, and wicking behavior of coated fabrics were evaluated in comparison with control fabric.

Fabric count was determined by following the ASTM D 3775 standard method. Yarn number in the warp and fill directions of the fabric was counted on a 25 × 25 mm area. Five randomly selected areas from each coated fabric were used to determine the average fabric count. These counts are summarized in Supporting Information Table S1 where the yarn numbers of 5 BL-coated fabrics in both directions are shown to be only 1.2% different from the control fabric. For the 20 BL-coated fabrics, the yarn number is less than 2.5% different in the warp direction, while in fill direction there is less than a 5% difference. These results demonstrate that the coating of polymer and clay layers on the fabric did not significantly alter its physical structure. Wet processing of cotton fabric with traditional textile fin-

TABLE 3. Tearing Force and Tensile Breaking Force of Uncoated and Coated Fabrics

		tearing force (lbs)		breaking force (lbs)		elongation (%)	
sample	BL number	warp	fill	warp	fill	warp	fill
control		2.11	2.02	66.30	69.34	19.5	30.7
BPEI pH10/0.2% MMT	5	2.26	1.99	72.92	68.09	15.7	38.5
	20	2.25	2.02	67.23	63.66	16.9	36.4
BPEI pH 7/0.2% MMT	5	2.24	2.12	80.33	65.88	14.7	36.8
	20	2.22	2.05	75.29	66.13	14.7	36.3
BPEI pH 10/1% MMT	5	2.21	1.86	80.11	61.54	12.1	30.1
	20	2.25	1.80	78.58	73.50	13.5	31.2
BPEI pH 7/1% MMT	5	2.29	2.01	71.35	66.43	12.8	31.1
	20	2.04	1.87	68.76	63.23	14.5	30.8

ishes often causes shrinkage and compaction in the yarns, resulting in more yarns per inch and affecting the comparison of physical properties of the treated fabrics to control materials.[53]

The Elmendorf tearing test, which uses a falling pendulum to determine the amount of force required to tear the fabric (ASTM D 1424), was used to evaluate tear strength. A strip tensile strength test was used to determine the maximum force that can be applied to a material (sampled as a strip) until it fractures (ASTM D 5035). Additionally, the strip test measures the apparent elongation of the fabric. The Elmendorf and tensile tests showed similar results, which are summarized in Table 3. The warp direction for the coated fabrics exhibited improvement in both tearing and breaking strength when compared to the control fabric, while the fill direction showed a general decrease in strength. The elongation results had slight directionality as well. The warp direction showed a decrease in elongation, while the fill direction showed an increase. All of these properties are within 10% of the uncoated fabric, so the data do not reveal a clear connection between coating and strength properties. The nature of these results suggest that they are not based on a change in fiber structure due to the coating, but rather are within the range of strength and elongation for the uncoated fabrics. In other words, the coating neither greatly improved nor harmed the fabric's mechanical strength. This is an improvement relative to traditional textile finishing that decreases the tensile strength of cotton fabric.[54]

The AATCC Committee RA63 proposed test method for wicking was used to test the transfer of water through the various fabric samples. Most standard fabrics absorb water through capillary action, using the gaps between warp and fill yarns as small capillaries, causing them to absorb a comparatively large amount of water. The wicking test measures the time it takes water to travel up a piece of fabric in an Erlenmeyer flask or beaker. Shorter wicking times (i.e., faster movement of water up the test strip) indicate better wicking ability. The wicking distance is 20 mm and wicking rates were calculated by dividing the wicking distances by the average wicking times. Wicking rates in the warp and fill directions of each fabric are summarized in Table S2 (see Supporting Information). For all coated fabrics, both warp and fill wicking rates are much slower (by a factor of 2−3) than the control fabric, indicating that their ability to absorb and transport water is not as great as the control. This is not so surprising, considering the outermost clay layer has been analyzed using *ab initio* molecular dynamics, where it was concluded that its tetrahedral surface (i.e., the oxygen plane, which is the widest dimension in MMT surface) can be considered hydrophobic.[55] In addition, static contact angle results were 72° for a coating of BPEI pH 7/1 wt % MMT on a Si wafer, and 74° for BPEI pH 10/1 wt % MMT, suggesting that the MMT-covered surface is more hydrophobic since both contact angles are larger than the 38° measured for a bare Si wafer. Among the four different types of fabric coatings studied here, the ones involving pH 7 BPEI have slower wicking rates than those made using pH 10, which suggests that it is harder for water to be transported through pH 7 BPEI coated fabrics. This behavior might be caused by the MMT platelets lying parallel to the fiber surface during deposition, with highly charged BPEI at pH 7 packing the platelets especially tightly. Such an arrangement of clay platelets, which are slightly hydrophobic, provide excellent coverage and sealing of fiber surfaces, thus interfering with the moisture transport both along and through the fiber. This is an area of ongoing research and improved wicking (if desired) could presumably be accomplished by applying a few bilayers of highly hydrophilic polymers.

CONCLUSIONS

This study focused on various BPEI/MMT thin film assemblies, with the goal of developing a flame-retardant coating system for cotton fabrics. Films assembled

with high or low pH polyethylenimine and 1 or 0.2 wt % clay suspensions all showed linear growth as a function of the number of BL deposited. Higher BPEI pH resulted in much thicker assemblies due to lower charge density. With respect to clay, using a higher concentration resulted in slightly thicker films. Flame-retardant properties of 5 and 20 BL coatings on cotton fabric were tested with TGA, vertical flame testing, and microcombustion calorimetry. A 7 to 13% residue was left over from coated fabric after heat treatment at 500 °C under an air atmosphere, whereas the control fabric completely combusted. This level of charring is significant, because the coating contributed only 1 to 4 wt % to the fabric (depending on recipe and number of layers) prior to burning. During actual burning in the vertical flame test, afterglow time was significantly reduced for the coated fabrics. The weave structure of the fabric, as observed in SEM images, was well preserved relatively to the chars from coated fabrics, whereas the scant ashes from the control fabric showed little structure. SEM also revealed that each individual yarn was protected by the sheath-like coating. Additionally, microcalorimeter testing revealed lower heat release for coated fabrics, suggesting that fewer combustible volatiles were generated. The physical properties of the fabrics did not show great differences between control and coated, suggesting that the coating does not adversely affect the desirable properties of the fabric itself. The simplicity of the layer-by-layer process provides a convenient method for imparting flame resistance to fabric using relatively benign ingredients. In addition to clays, other types of flame-retardant particles and polymers could be considered for use in these types of coatings. To this end, further studies are currently under way to further reduce the flammability of cotton and other commonly used fabrics.

METHODS

Preparation of Deposition Mixtures. Cationic deposition solutions were prepared by dissolving 0.1 wt % branched polyethylenimine, with a molecular weight of 25 000 g/mol (Aldrich, Milwaukee, WI), into 18.2 MΩ deionized water from a Direct-QTM 5 ultrapure water system (Millipore, Billerica, MA). The unadjusted pH of this solution is 10.3, but this value was adjusted to 7 and 10 by adding 1 M hydrochloric acid (36.5−38.0% HCl; Mallinckrodt Chemicals, Phillipsburg, NJ). Sodium montmorillonite, trade name Cloisite Na^+ (Southern Clay Products, Inc., Gonzales, TX), was exfoliated by simply adding it to deionized water (0.2 or 1.0 wt %) and slowly rolling for 24 h, to produce the anionic deposition mixtures. MMT has a cationic exchange capacity of 0.926 meq/g and a negative surface charge in deionized water.[56] Individual platelets have a density of 2.86 g/cm^3, with a planar dimension of 10−1000 nm (average is around 200 nm) and a thickness of 1 nm.[57] The pH was measured with an Accumet Basic AB15 pH meter (Fisher Scientific, Pittsburgh, PA).

Substrates. Single-side-polished silicon wafers (University Wafer, South Boston, MA) were used as deposition substrates for films characterized by ellipsometry and AFM. Polished Ti/Au crystals with a resonance frequency of 5 MHz were purchased from Maxtek, Inc. (Cypress, CA) and used as deposition substrates for quartz crystal microbalance characterization. TEM imaging of these films required the use of 125 μm polystyrene (PS) film (Goodfellow, Oakdale, PA) as the substrate for deposition. Prior to deposition, silicon wafers were rinsed with acetone, then deionized water, and finally dried with filtered air. In the case of PS substrates, the film was rinsed with methanol and deionized water, and dried with air. The clean PS substrates were then corona-treated with a BD-20C Corona Treater (Electro-Technic Products Inc., Chicago, IL) for 2 min. Corona treatment oxidizes the PS film surface and creates a negative surface charge,[58,59] which improves adhesion of the first BPEI layer. Scoured and bleached plain-woven cotton fabric, that was coated and tested for thermal stability, was supplied by the United States Department of Agriculture (USDA) Southern Regional Research Center (SRRC, New Orleans, LA). The fabric was a balanced weave with approximately 80 threads per inch in both the warp and fill direction, with a weight of 119 g/m^2. The control fabric referred to in this paper was treated by laundering through a cold water cycle, with no detergent, in a standard commercial high-efficiency clothes washer and dried for approximately 30 min in a commercial electric clothes dryer (Whirlpool Corporation, Benton Harbor, MI). The wet processing of the control fabric was intended to eliminate any changes in physical construction of the fabric due to the wet processing of the fabric during the LbL deposition. This wet-processed fabric was used as the uncoated fabric in all tests.

Layer-by-Layer Deposition. All films were assembled on a given substrate using the procedure shown in Figure 11. Each substrate was dipped into the ionic deposition mixtures, alternating between the BPEI (cationic) and MMT (anionic), with each cycle corresponding to one bilayer. The first dip into each mixture was for 5 min, beginning with the cationic solution. Subsequent dips were for 2 min each. Every dip was followed by rinsing with deionized water and drying with a stream of filtered air for 30 s each. In the case of the fabrics, the drying step involved wringing the water out instead of air-drying. After achieving the desired number of bilayers, the coated wafers were dried with filtered air, whereas the fabrics were dried in an 80 °C oven for 2 h.

Film Growth Characterization. Film thickness was measured on silicon wafer using a PhE-101 discrete wavelength ellipsometer (Microphotonics, Allentown, PA). The HeNe laser (632.8 nm) was set at an incidence angle of 65°. A Maxtek Research Quartz Crystal Microbalance (QCM) from Infinicon (East Syracuse, NY), with a frequency range of 3.8−6 MHz, was used in conjunction with 5 MHz quartz crystals to measure the weight per deposited layer. The crystal, in its holder, was dipped alternately into the positively and negatively charged solutions. Between each dip, the crystal was rinsed, dried, and left on the microbalance for 5 min to stabilize. Cross sections of the clay−polymer assemblies were imaged with a JEOL 1200 EX TEM (Mitaka, Tokyo, Japan), operated at 110 kV. Samples were prepared for imaging by embedding a piece of coated PS in epoxy and sectioning it with a microtome equipped with a diamond knife. Surface structures were imaged with a Nanosurf EasyScan 2 atomic force microscope (AFM) (Nanoscience Instruments, Inc., Phoenix, AZ). AFM images were gathered in tapping mode with a XYNCHR cantilever tip. A Bruker-AXS D8 Advanced Bragg−Brentano X-ray powder diffractometer (Cu Kα, λ = 1.541 Å) (Bruker AXS Inc., Madison, WI) was used for both powder diffraction and glancing angle XRD. Contact angle measurements were done using a CAM 200 optical contact angle meter (KSV Instruments Ltd., Helsinki, Finland).

Thermal, Flammability, and Combustibility Testing. All tests were conducted in triplicate for each system to obtain the reported averages. The thermal stability of uncoated and coated fabrics was measured in a Q50 thermogravimetric analyzer (TA Instruments, New Castle, DE). Each sample was approximately 20 mg and was tested in an air atmosphere, from room temperature to 600 °C, with a heating rate of 20 °C/min. Vertical flame testing was performed on 3 × 12 in. sections of uncoated and coated fabrics according to ASTM D6413. An automatic vertical flammability cabinet, model VC-2 (Govmark, Farmingdale, NY), was used

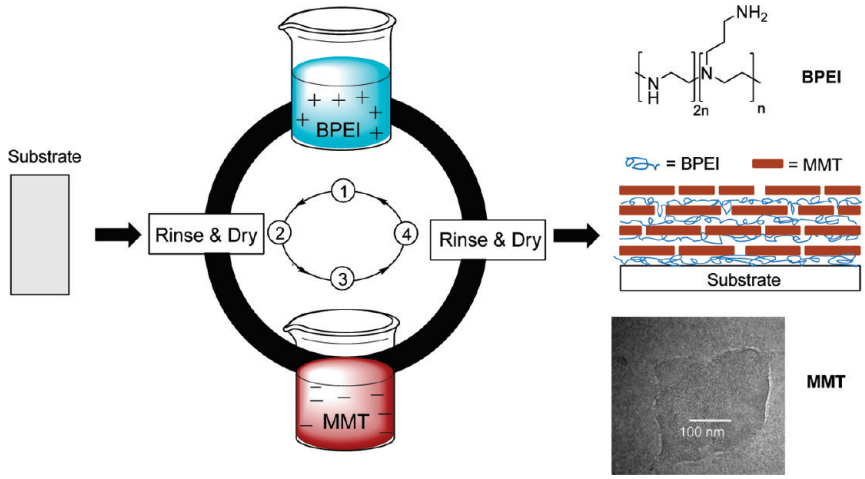

Figure 11. Schematic of the LbL deposition process used to prepare clay-BPEI assemblies. Steps 1−4 are repeated until the desired number of bilayers are deposited. The TEM image of MMT shown here is reprinted from ref 57. Copyright 2006 American Chemical Society.

to conduct this testing. The Bunsen burner flame, 19 mm below the fabric sample, was applied for 12 s, after which the afterflame and after-glow times were measured. Microscale combustibility experiments were carried out in a Govmark MCC-1 microscale combustion calorimeter.[60] The specimens were first kept at 100 °C for 5 min to remove adsorbed moisture, and then heated up to 700 °C at a heating rate of 1 °C/sec, in a stream of nitrogen flowing at 80 cm^3/min. The pyrolysis volatiles released from the thermal degradation of the sample into the nitrogen gas stream were mixed with a 20 cm^3/min stream of pure oxygen prior to entering a 1000 °C combustion furnace. Three samples weighing about 4.3 mg were tested for each system.

Analysis of Fabric Properties. Surface images of control and coated fabrics, as well as afterburn chars (after direct exposure to flame), were acquired with a Quanta 600 FE-SEM (FEI Company, Hillsboro, OR). Physical properties of the fabric were tested at USDA-SRRC using ASTM and AATCC (American Association of Textile Chemists and Colorists) Standards. ASTM D 3775 was used to determine the fabric count on the fabric sample, counting the number of yarns in the warp and fill directions at five different locations to determine the average number of yarns per inch. ASTM D 1424 was used to determine the fabric's resistance to tearing. This test was carried out using the Elmendorf falling pendulum apparatus (SDL Atlas, Stockport, UK). Two clamps secured the sample and a slit was cut down the center before a pendulum action attempted to tear the fabric. Control samples were tested five times and coated samples were tested three times due to insufficient material to allow for five test specimens. ASTM D 5035 was used to determine the breaking force and percent of apparent elongation. A sample piece of fabric was placed in a constant-rate-of-extension tensile testing machine and a force was applied until the sample broke (Instron Corporation, Norwood, MA). As with the Elmendorf test, control samples were tested five times and coated samples were tested three times. To determine water-wicking ability, the AATCC Committee RA63 proposed test method for wicking was employed. A 25 mm ×175 mm strip of fabric was placed in a beaker with water, and the time it took the water to climb 2 cm vertically was measured. All fabrics were preconditioned at 21 °C and 65% RH (according to ASTM D 1776) for 48 h before testing.

Acknowledgment. The authors would like to acknowledge the Building and Fire Research Laboratory (BFRL) at the National Institute of Standards and Technology (NIST) for financial support of this work. The authors also thank Dr. Y. S. Kim for assistance with SEM imaging.

Supporting Information Available: The postburn images of vertical flame testing of uncoated and coated fabrics, tables of fabric counts, and wicking rate. This material is available free of charge *via* the Internet at http://pubs.acs.org.

REFERENCES AND NOTES

1. Karter, M. J., Jr. NFPA Reports: U.S. Fire Loss for 2007. *Natl. Fire Protect. Assoc. J.* September/October 2008.
2. Kensley, J. N. Learning from Mistakes. *Chem. Eng. News* **2009**, *87*, 59.
3. Wakelyn, P. J.; Bertoniere, N. R.; French, A. D.; Thibodeaux, D. *Cotton Fiber Chemistry and Technology*; CRC Press (Taylor and Francis Group): Boca-Raton, FL, 2007; p 77−80.
4. Oulton, D. P. Fire-Retardant Textiles. In *Chemistry of the Textiles Industry*; Carr, C. M., Ed.; Springer-Verlag: Berlin, 1995; Chapter 3.
5. Martin, C.; Ronda, J. C.; Cadiz, V. Boron-Containing Novolac Resins as Flame Retardant Materials. *Polym. Degrad. Stab.* **2006**, *91*, 747–754.
6. Sather, J. M.; Richards, H. R. Efficiency of Phosphorus-Containing Compounds for Inhibiting Afterglow in Cellulose Fabrics. *Am. Dyestuff Rep.* **1970**, *59*, 21–26.
7. Yang, C. Q.; Wu, W. D.; Xu, Y. The Combination of a Hydroxy-Functional Organophosphorus Oligomer and Melamine-Formaldehyde as a Flame Retarding Finishing System for Cotton. *Fire Mater.* **2005**, *29*, 109–120.
8. Horrocks, A. R.; Kandola, B. K.; Smart, G.; Zhang, S.; Hull, T. R. Polypropylene Fibers Containing Dispersed Clays Having Improved Fire Performance. I. Effect of Nanoclays on Processing Parameters and Fiber Properties. *J. Appl. Polym. Sci.* **2007**, *106*, 1707–1717.
9. Bourbigot, S.; Devaux, E.; Flambard, X. Flammability of Polyamide-6/Clay Hybrid Nanocomposite Textiles. *Polym. Degrad. Stab.* **2002**, *75*, 397–402.
10. Solarski, S.; Ferreira, M.; Devaux, E.; Fontaine, G.; Bachelet, P.; Bourbigot, S.; Delobel, R.; Coszach, P.; Murariu, M.; Ferreira, A. D. S.; *et al*. Designing Polylactide/Clay Nanocomposites for Textile Applications: Effect of Processing Conditions, Spinning, and Characterization. *J. Appl. Polym. Sci.* **2008**, *109*, 841–851.
11. Devaux, E.; Rochery, M.; Bourbigot, S. Polyurethane/Clay and Polyurethane/POSS Nanocomposites as Flame Retarded Coating for Polyester and Cotton Fabrics. *Fire Mater.* **2002**, *26*, 149–154.
12. Liu, Y. Y.; Wang, X. W.; Qi, K. H.; Xin, J. H. Functionalization of Cotton with Carbon Nanotubes. *J. Mater. Chem.* **2008**, *18*, 3454–3460.
13. Zanetti, M.; Kashiwagi, T.; Falqui, L.; Camino, G. Cone Calorimeter Combustion and Gasification Studies of Polymer Layered Silicate Nanocomposites. *Chem. Mater.* **2002**, *14*, 881–887.
14. Kashiwagi, T.; Du, F. M.; Douglas, J. F.; Winey, K. I.; Harris, R. H.; Shields, J. R. Nanoparticle Networks Reduce the Flammability of Polymer Nanocomposites. *Nat. Mater.* **2005**, *4*, 928–933.

15. Ariga, K.; Hill, J. P.; Ji, Q. Layer-by-Layer Assembly as a Versatile Bottom-Up Nanofabrication Technique for Exploratory Research and Realistic Application. *Phys. Chem. Chem. Phys.* **2007**, *9*, 2319–2340.
16. Decher, G. Polyelectrolyte Multilayers, an Overview. In *Multilayer Thin Films: Sequential Assembly of Nanocomposite Materials*; Decher, G.; Schlenoff, J. B., Eds.: Wiley-VCH: Weinheim, Germany, 2003; Chapter 1.
17. Bertrand, P.; Jonas, A.; Laschewsky, A.; Legras, R. Ultrathin Polymer Coatings by Complexation of Polyelectrolytes at Interfaces: Suitable Materials, Structure and Properties. *Macromol. Rapid Commun.* **2000**, *21*, 319–348.
18. Podsiadlo, P.; Shim, B. S.; Kotov, N. A. Polymer/Clay and Polymer/Carbon Nanotube Hybrid Organic-Inorganic Multilayered Composites Made by Sequential Layering of Nanometer Scale Films. *Coord. Chem. Rev.* **2009**, *253*, 2835–2851.
19. Bergbreiter, D. E.; Tao, G. L.; Franchina, J. G.; Sussman, L. Polyvalent Hydrogen-Bonding Functionalization of Ultrathin Hyperbranched Films on Polyethylene and Gold. *Macromolecules* **2001**, *34*, 3018–3023.
20. Lv, F.; Peng, Z. H.; Zhang, L. L.; Yao, L. S.; Liu, Y.; Xuan, L. Photoalignment of Liquid Crystals in a Hydrogen-Bonding-Directed Layer-by-Layer Ultrathin Film. *Liq. Cryst.* **2009**, *36*, 43–51.
21. Shimazaki, Y.; Nakamura, R.; Ito, S.; Yamamoto, M. Molecular Weight Dependence of Alternate Adsorption through Charge-Transfer Interaction. *Langmuir* **2001**, *17*, 953–956.
22. Sun, J. Q.; Wu, T.; Liu, F.; Wang, Z. Q.; Zhang, X.; Shen, J. C. Covalently Attached Multilayer Assemblies by Sequential Adsorption of Polycationic Diazoresins and Polyanionic Poly(acrylic acid). *Langmuir* **2000**, *16*, 4620–4624.
23. Bergbreiter, D. E.; Chance, B. S. "Click"-Based Covalent Layer-by-Layer Assembly on Polyethylene Using Water-Soluble Polymeric Reagents. *Macromolecules* **2007**, *40*, 5337–5343.
24. Mermut, O.; Barrett, C. J. Effects of Charge Density and Counterions on the Assembly of Polyelectrolyte Multilayers. *J. Phys. Chem. B* **2003**, *107*, 2525–2530.
25. Zhang, H. N.; Ruhe, J. Interaction of Strong Polyelectrolytes with Surface-Attached Polyelectrolyte Brushes−Polymer Brushes as Substrates for the Layer-by-Layer Deposition of Polyelectrolytes. *Macromolecules* **2003**, *36*, 6593–6598.
26. Sui, Z.; Salloum, D.; Schlenoff, J. B. Effect of Molecular Weight on the Construction of Polyelectrolyte Multilayers: Stripping *versus* Sticking. *Langmuir* **2003**, *19*, 2491–2495.
27. McAloney, R. A.; Sinyor, M.; Dudnik, V.; Goh, M. C. Atomic Force Microscopy Studies of Salt Effects on Polyelectrolyte Multilayer Film Morphology. *Langmuir* **2001**, *17*, 6655–6663.
28. Chang, L.; Kong, X.; Wang, F.; Wang, L.; Shen, J. Layer-by-Layer Assembly of Poly(*N*-acryloyl-*N*′-propylpiperazine) and Poly(acrylic acid): Effect of pH and Temperature. *Thin Solid Films* **2008**, *516*, 2125–2129.
29. Shiratori, S. S.; Rubner, M. F. pH-Dependent Thickness Behavior of Sequentially Adsorbed Layers of Weak Polyelectrolytes. *Macromolecules* **2000**, *33*, 4213–4219.
30. Tan, H. L.; McMurdo, M. J.; Pan, G. Q.; Van Patten, P. G. Temperature Dependence of Polyelectrolyte Multilayer Assembly. *Langmuir* **2003**, *19*, 9311–9314.
31. Fu, J. H.; Ji, J.; Fan, D. Z.; Shen, J. C. Construction of Antibacterial Multilayer Films Containing Nanosilver *via* Layer-by-Layer Assembly of Heparin and Chitosan-Silver Ions Complex. *J. Biomed. Mater. Res. A* **2006**, *79A*, 665–674.
32. Dvoracek, C. M.; Sukhonosova, G.; Benedik, M. J.; Grunlan, J. C. Antimicrobial Behavior of Polyelectrolyte-Surfactant Thin Film Assemblies. *Langmuir* **2009**, *25*, 10322–10328.
33. Hiller, J.; Mendelsohn, J. D.; Rubner, M. F. Reversibly Erasable Nanoporous Antireflection Coatings from Polyelectrolyte Multilayers. *Nat. Mater.* **2002**, *1*, 59–63.
34. Park, Y. T.; Grunlan, J. C. Fast Switching Electrochromism from Colloidal Indium Tin Oxide in Tungstate-Based Thin Film Assemblies. *Electrochim. Acta* **2010**, *55*, 3257–3267.
35. Choi, K.; Yoo, S. J.; Sung, Y. E.; Zentel, R. High Contrast Ratio and Rapid Switching Organic Polymeric Electrochromic Thin Films Based on Triarylamine Derivatives from Layer-by-Layer Assembly. *Chem. Mater.* **2006**, *18*, 5823–5825.
36. Jain, V.; Sahoo, R.; Jinschek, J. R.; Montazami, R.; Yochum, H. M.; Beyer, F. L.; Kumar, A.; Heflin, J. R. High Contrast Solid State Electrochromic Devices Based on Ruthenium Purple Nanocomposites Fabricated by Layer-by-Layer Assembly. *Chem. Commun.* **2008**, 3663–3665.
37. He, Q.; Cui, Y.; Li, J. B. Molecular Assembly and Application of Biomimetic Microcapsules. *Chem. Soc. Rev.* **2009**, *38*, 2292–2303.
38. Priolo, M. A.; Gamboa, D.; Grunlan, J. C. Transparent Clay−Polymer Nano Brick Wall Assemblies with Tailorable Oxygen Barrier. *ACS Appl. Mater. Interfaces* **2010**, *2*, 312–320.
39. Yu, H. H.; Cao, T.; Zhou, L. D.; Gu, E. D.; Yu, D. S.; Jiang, D. S. Layer-by-Layer Assembly and Humidity Sensitive Behavior of Poly(ethyleneimine)/Multiwall Carbon Nanotube Composite Films. *Sens. Actuators, B* **2006**, *119*, 512–515.
40. Everett, W. N.; Jan, C. J.; Sue, H. J.; Grunlan, J. C. Micropatterning and Impedance Characterization of an Electrically Percolating Layer-by-Layer Assembly. *Electroanalysis* **2007**, *19*, 964–972.
41. Aoki, P. H. B.; Volpati, D.; Riul, A.; Caetano, W.; Constantino, C. J. L. Layer-by-Layer Technique as a New Approach to Produce Nanostructured Films Containing Phospholipids as Transducers in Sensing Applications. *Langmuir* **2009**, *25*, 2331–2338.
42. Ras, R. H. A.; Umemura, Y.; Johnston, C. T.; Yamagishi, A.; Schoonheydt, R. A. Ultrathin Hybrid Films of Clay Minerals. *Phys. Chem. Chem. Phys.* **2007**, *9*, 918–932.
43. Ou, R. Q.; Zhang, J. G.; Deng, Y. L.; Ragauskas, A. J. Polymer Clay Self-Assembly Complexes on Paper. *J. Appl. Polym. Sci.* **2007**, *105*, 1987–1992.
44. Tang, Z. Y.; Wang, Y.; Podsiadlo, P.; Kotov, N. A. Biomedical Applications of Layer-by-Layer Assembly: From Biomimetics to Tissue Engineering. *Adv. Mater.* **2006**, *18*, 3203–3224.
45. Lutkenhaus, J. L.; Olivetti, E. A.; Verploegen, E. A.; Cord, B. M.; Sadoway, D. R.; Hammond, P. T. Anisotropic Structure and Transport in Self-Assembled Layered Polymer−Clay Nanocomposites. *Langmuir* **2007**, *23*, 8515–8521.
46. Podsiadlo, P.; Kaushik, A. K.; Arruda, E. M.; Waas, A. M.; Shim, B. S.; Xu, J.; Nandivada, H.; Pumplin, B. G.; Lahann, J.; Ramamoorthy, A.; Kotov, N. A. Ultrastrong and Stiff Layered Polymer Nanocomposites. *Science* **2007**, *318*, 80–83.
47. Podsiadlo, P.; Michel, M.; Lee, J.; Verploegen, E.; Kam, N. W. S.; Ball, V.; Lee, J.; Qi, Y.; Hart, A. J.; Hammond, P. T.; Kotov, N. A. Exponential Growth of LBL Films with Incorporated Inorganic Sheets. *Nano Lett.* **2008**, *8*, 1762–1770.
48. Li, Y.-C.; Schulz, J.; Grunlan, J. C. Polyelectrolyte/Nanosilicate Thin-Film Assemblies: Influence of pH on Growth, Mechanical Behavior, and Flammability. *ACS Appl. Mater. Interfaces* **2009**, *1*, 2338–2347.
49. Vertlib, V.; Dietiker, M.; Plotze, M.; Yezek, L.; Spolenak, R.; Puzrin, A. M. Fast Assembly of Bio-inspired Nanocomposite Films. *J. Mater. Res.* **2008**, *23*, 1026–1035.
50. Schartel, B.; Pawlowski, K. H.; Lyon, R. E. Pyrolysis Combustion Flow Calorimeter: A Tool to Assess Flame Retarded PC/ABS Materials. *Thermochim. Acta* **2007**, *462*, 1–14.
51. Lyon, R. E.; Walters, R. N. Pyrolysis Combustion Flow Calorimetry. *J. Anal. Appl. Pyrolysis* **2004**, *71*, 27–46.
52. Hergenrother, P. M.; Thompson, C. M.; Smith, J. G.; Connell, J. W.; Hinkley, J. A.; Lyon, R. E.; Moulton, R. Flame Retardant Aircraft Epoxy Resins Containing Phosphorus. *Polymer* **2005**, *46*, 5012–5024.
53. Suh, M. W. A Study of Shrinkage of Plain Knitted Cotton Fabric Based on Structural Changes of Loop Geometry

Due to Yarn Swelling and Deswelling. *Text. Res. J.* **1967**, *37*, 417–431.
54. Zeronian, S. H.; Bertoniere, N. R.; Alger, K. W.; Duffin, J. L.; Kim, M. S.; Dubuque, L. K.; Collins, M. J.; Xie, C. Effect of Dimethyloldihydroxyethyleneurea on the Properties of Cellulosic Fibers. *Text. Res. J.* **1989**, *59*, 484–492.
55. Tunega, D.; Gerzabek, M. H.; Lischka, H. *Ab initio* Molecular Dynamics Study of a Monomolecular Water Layer on Octahedral and Tetrahedral Kaolinite Surfaces. *J. Phys. Chem. B* **2004**, *108*, 5930–5936.
56. Annabi-Bergaya, F. Layered Clay Minerals. Basic Research and Innovative Composite Applications. *Microporous Mesoporous Mater.* **2008**, *107*, 141–148.
57. Ploehn, H. J.; Liu, C. Y. Quantitative Analysis of Montmorillonite Platelet Size by Atomic Force Microscopy. *Ind. Eng. Chem. Res.* **2006**, *45*, 7025–7034.
58. Owens, D. K. The Mechanism of Corona and Ultraviolet Light-Induced Self-Adhesion of Poly(ethylene terephthalate) Film. *J. Appl. Polym. Sci.* **1975**, *19*, 3315–3326.
59. Zhang, D.; Sun, Q.; Wadsworth, L. C. Mechanism of Corona Treatment on Polyolefin Films. *Polym. Eng. Sci.* **1998**, *38*, 965–970.
60. Combustibility testing was carried out by the National Institute of Standards and Technology (NIST), an agency of the US government and by statute is not subject to copyright in USA. The identification of any commercial product or trade name does not imply endorsement or recommendation by NIST. The policy of NIST is to use metric units of measurement in all its publications, and to provide statements of uncertainty for all original measurements. In this document, however, data from organizations outside NIST are shown, which may include measurements in non-metric units or measurements without uncertainty statements.